Evaluating local geological conditions and *Vs* profiles in Khash area, SE Iran

Ebrahim Rahimi
Department of Engineering Geology, Tarbiat Modares University, Tehran, Iran
Tel: +98-912-216-3028 E-mail: rahimi_e@modares.ac.ir

Mohammad Reza Nikoudel (Corresponding author)
Department of Engineering Geology, Tarbiat Modares University, Tehran
PO Box: 14115-175, Tehran, Iran
Tel: +98-912-105-6145 E-mail: nikudelm@modares.ac.ir

Naser Hafezi Moghaddas
Department of Engineering Geology, Ferdowsi University, Mashhad, Iran
E-mail: moghaddas@shahrudut.ac.ir

Mohammad Reza Ghayamghamian
International Institute of Earthquake Engineering and Seismology (IIEES), Tehran, Iran
E-mail: mrgh@iiees.ac.ir

Abstract

Local geological condition and site dynamic parameters especially shear wave velocity (*Vs*) are of great importance in designing safe structures and prohibition or reduction earthquake disasters particularly in populated cities. Iranian eastern cities, located on young sediments and having moderate to high seismicity potential, have been subjected to seismic hazards and have been involved in pertinent studies. In this regard, in the absence of adequate information for Khash area, SE Iran, a reconnaissance campaign—including geological, geotechnical and seismic downhole surveys— was carried out, to characterize the site and to provide a setting for detailed microtremors surveys aimed at assessing site effects and *Vs* structure. Accordingly, site geology was studied. Using seismic downhole surveys *Vs* structures were obtained in 6 boreholes based of which the ground was classified as class C and II in terms of the NEHRP provisions and Iranian code of practice, respectively. Microtremors were measured at 85 stations and were analyzed using H/V technique. Three different shapes of the H/V curves were recognized and their spatial distributions were mapped. The analysis shows a resonance period range of 0.4-1.54 s and a quasi-amplitude range of 1.8 to 7.0. It is shown that the *Vs30*-based classes of the site differ from the period-based classes, indicating that herein the *Vs30* is not sufficient for site amplification, as mentioned by other authors. By inverting H/V curves, we obtained 11 1-D velocity models using ModelHVSR program. These *Vs* models that are related to the sites having rather high amplitudes and clear peaked curves are comparable to what obtained by downholes.

Keywords: Khash area, Microtremor H/V, *Vs* profile, ModelHVSR.

1. Introduction

Iran is one of the most seismically active regions in the world that has experienced several catastrophic earthquakes, for example: Tabas 1978 (7.8 M_L), Manjil–Rudbar 1990 (7.4 M_w) and Bam 2003 (6.6 M_w). Iranian eastern cities have located in a moderate to high seismic region on young sediments and are prone to seismic hazards. Nevertheless, they have received less attention and the limited available information is not reliable for engineering purposes, so they have been currently involved in pertinent studies. This study is the first attempt to provide Khash city, SE Iran, with site effect information.

When civil engineering projects are based on limited geological or geotechnical information, misinterpretations and undesirable problems frequently arise and the projects suffer cost increases and delays. Furthermore, for the ground and structures located in seismic prone areas, it is necessary to grasp their seismic characteristics precisely in advance (Nakamura, 1997). Thus, for every civil project, obtaining subsurface characteristics is a vital issue that is usually done by drilling boreholes. In spite of valuable and precise information obtained by this technique, it is time-consuming, expensive, and extremely localized. As an alternative, geophysical surveying provides a relatively rapid and cost-effective means of deriving areally distributed information on subsurface geology (Delgado et al., 2000; Kearey et al., 2002). Today, the developed methods based on microtremors are used as useful techniques to provide the study with more data that are traditionally obtained from borings and/or geological-seismic surveys. Microtremors (ambient seismic noises) are low amplitude vibrations generated by natural disturbances such as wind, sea tides or by man-made origins such as traffic, industrial machinery, household appliances, etc. It is shown that the fundamental resonance frequency of the subsoil can be directly derived by microtremor observation. These methods have been employed for gathering a variety of parameters such as depth to bedrock, *Vs* profile, underground heterogeneity, etc. as well (Konno and Ohmachi, 1998; Parolai and Galiana-Merino, 2006; Ibs-Von Seht and Wohlenberg, 1999).

Among the several techniques proposed for the estimation of the site response indicators such as fundamental frequencies and amplification factors, the Nakamura technique (also known as Horizontal to Vertical spectral Ratio technique: HVSR or H/V) is widely used. The technique originally proposed by Nogoshi and Igarashi (1971), and wide-spread by Nakamura (1989), consists of estimating the ratio between the Fourier amplitude spectra of the horizontal (H) to vertical (V) components of microtremors recorded at one single station. This is a powerful and efficient tool due to its simplicity, low cost and the rather short time needed for measurement and processing and interpretation, which allows detailed mapping of local site effects in an urban area even without knowing precise subsurface geological and S-wave structures (Field et al., 1990; Lermo and Chavez-Garcia, 1993; Lachet and Bard, 1994; Field and Jacob, 1995; Parolai et al., 2001; Ghayamghamian et al., 2007, Picozzi et al., 2009).

Some researchers have tried to apply the H/V's to extract *Vs* structures of sediments. Two different hypotheses are followed for such evaluations. A hypothesis is that H/V is basically related to the ellipticity of the fundamental mode of Rayleigh waves that composes the noise. One can invert the H/V peak frequencies to derive the S-wave velocity profiles (Fäh et al., 2003). Another hypothesis is that the body-waves compose the noise. ModelHVSR® program developed by Herak (2008) is based on the later hypothesis. Two assumptions, i.e. horizontal layering and vertical incidence should be kept in mind during using this program; otherwise the results might contain some mistake.

As this study is the first to describe the geological and geophysical conditions of Khash area, we tried to characterize the area with various techniques and to provide the basin with much more data. However, we mainly focused on deriving the local geological condition and the shear wave velocity structures of Khash basin. Summarily, using field works, geotechnical borings and seismic downhole survey, the geological conditions were evaluated and the *Vs30*-based site classes were determined. Microtremors were measured at 85 stations and using H/V analyses site effect proxies were mapped. Finally, we attempted to invert of the H/V's with the purpose of deriving the S-wave velocity profiles for the basin. So, by using the program ModelHVSR the shear wave velocity structures of the basin were obtained at some microtremor stations and the results were compared by the available downholes results.

2. Geological and seismotectonic setting

Khash city, with 60,000 inhabitants, lies about 45 kms south of the dormant stratovolcano of Taftan, within latitudes 61° 4.8′ N and 62° 20.9′ N and longitudes 28° 4.8′ E and 28° 21.6′ E, in the core of an eroded anticline. Our

seismotectonic study conducted over this area (not mentioned here) shows that for a recurrence interval of 100 years, the probability of occurrence of earthquakes with magnitude of 5.6 - 6.5 is more than 90%. Except the report of 1:100,000-scale geological map of Khash (Fig.1) (Shahrabi, 1995), there is no integrated study to define the valley geometry and geology. The scarcity of information especially drilling or geophysical data suppresses us to make out a detailed subsurface geology. This study can be a starting point for future detail studies. We updated and re-built the available map on the basis of satellite images and field observations. Figure 2 depicts a simplified geological section map along the west-east of the valley. As seen, the valley is situated on the core of an eroded anticline whose current limbs make the western and eastern heights. The morphology of the study area corresponds to an intermountain basin or wide valley with about 1420-masl for the ground surface and maximum height of 2100-masl for the adjacent heights. The main criteria for the sitting of the city in the area are availability of water and silty areas which are frequently cultivated when not covered by too much sand. These silty areas are thought to be partly waterlain and partly loessic. Many of the higher ridges have scree deposits "Q^{s}" which pass into younger fans "Q^{t2}".

The older rocks in the zone are of Eocene age. They are composed of limestone, marl, calcareous shale, and sandstone. The valley is filled by alluvial sediments deposited as terraces during accumulation-erosion cyclic changes. According to Figure 2, the city is mainly founded on quaternary sediments. The early quaternary sediments (Q^{t1}) including limestone and volcanic large clasts such as boulders or cobbles have been well cemented and deposited on the older sediments. Late quaternary sediments (Q^{t2}) that form the alluvial fan and terraces have covered a large part of the area. In the western and south western hillsides, these sediments have cut early sediments and covered them. The drainages and floodways basin surfaces have been covered by the recent sediments (Q^{al}). In the western and eastern hillsides, two floodways are seen whose relatively large widths indicate their active flooding conditions. In the southern and eastern parts of the valley several qanats (manmade underground water channels with vertical shafts) are terminated by the urban area.

Folding trends are NW-SE with dominant plunge to the SE. The limestone ridges, east of Khash, contain excellent examples of doubly plunging folds. Also, in east of Khash thrusting occurs in the limestone ridges with thrust planes dipping NE suggesting overthrusting from the NE or, alternatively, underthrusting from the SW. Faulting occurs extensively on the NW-SE trend and is generally dextral in its apparent movement. However, it is not possible to entirely separate the processes of tectonism and sedimentation in the sheet area.

3. Geotechnical and geophysical aspects

Almost for every subsurface geological exploration, the drilling is the most common approach. To correctly characterize the subsurface condition, six drillings were done with different depths - up to 40 m. Figure 3 shows the layout of the drilled boreholes on a prepared surface geology map. Due to the limitations in urban areas and financial problems, these boreholes are neither evenly distributed in the city nor sufficient for a detailed subsurface exploration. Besides, only four in-situ and ex-situ tests were done at some depths: particle size distribution, Atterberg limit, consolidation test, shear strength tests and Standard Penetration Test (SPT). For the civil construction purposes, the shear strength parameters, c and φ, were done only for the depths 2-5 m (Table 1). As seen from the N_{SPT} values, the overall soil strength is high. Figure 4 depicts six geotechnical borehole logs. No borehole reached bedrock.

According to the logs corroborated by the surface geological investigations including rivers cuts and their pattern system, three major surficial geological units were inferred with differing geological and geotechnical properties as follows: Fine to coarse grained sediments that consist of relatively coarse grained sediments from the hillsides to fine grains in the central part of the city; Bedrock that varies from sandstone to shale layers at different localities; A dense and cemented silty layer (8–28 m with N_{SPT}>50) along the boreholes BH2 and BH5 in the northern parts that continues towards the BH3 and BH6. This layer is considered as a chalky layer underlain by softer layers. In a general trend, moving from the central part of the site towards the directions east and west, the subsurface structure gets shallower, because the plain faces the mountains. Moving from the northwest parts (i.e. in the vicinity of the sediment sources) towards the southeast, the soil texture decreases in size.

Since mere geological characterizations are not sufficient to define a soil model useful for the site response analyses, some other parameters should be involved. It is well known that the shear wave velocity (*Vs*) is very important in seismic wave amplification, so it has been frequently used in designing models for the site response simulation and

the earthquake recordings interpretation (Apostolidis et al., 2006), as well as design applications and building codes (Kramer, 1996; Lang and Schwartz, 2006). A number of geophysical methods have been proposed for the near-surface site characterization and measuring the shear wave velocity using a variety of testing configurations, processing techniques, and inversion algorithms (Anbazhagan et al., 2008). Uphole, downhole, crosshole and suspension PS-logging are of current invasive and active source techniques for estimating Vs. Other techniques such as seismic refraction, reflection and SASW are common noninvasive and active source techniques. In addition, the developed passive source techniques based on ambient noise arrays (SPAC, FK or ReMi) have reached a consensus.

Downhole seismic survey is the simplest and cheapest method in the suite of borehole seismic techniques requiring only a single borehole. In this technique, an impulse source of energy is generated at the ground surface near the top of the borehole in which one or multiple geophones are lowered at the predetermined depths. Travel time of the body waves (S- and P-waves) between each geophone and the source is recorded. Recorded travel time is then plotted versus depth as in the seismic refraction test. These plots are then used to determine the maximum compression and shear wave velocities, *V*p and *Vs* of all soil layers (Woods, 1994; Luna and Jadi, 2000).

In earthquake geotechnical practice, the shear wave velocity is often expressed in terms of the average shear wave velocity of the upper 30 m (*Vs30*)—a widely used parameter to predict the potential amplification of seismic shaking (Holzer et al., 2005), based of which many building codes have been developed, such as NEHRP (BSSC, 2001) and Iranian standard 2800. Regarding the overburden thickness from borehole data, the average shear wave velocity *Vs*D for the depth D is written as:

$$VsD=\frac{\sum_{i=1}^{N} d_i}{\sum_{i=1}^{N} (d_i/v_i)} \quad (1)$$

where d_i and v_i denote the thickness in meter and the shear wave velocity in m/s (at a shear strain level of 10^{-5} or less) of the *i*th formation or layer, respectively, in a total of *N* layers, existing in the top D meter (Borcherdt, 1994; Williams et al., 2003).

In present study, downhole seismic tests were done at six available boreholes. The resulted *Vs* profiles (i.e., *Vs*'s versus depths) are presented at one graph in Figure 5*a*. The final survey depth and maximum/minimum *Vs* values are 35 m, 115 m/s and 800 m/s, respectively. It is custom to correlate *Vs* with some soil indexes such as N_{SPT}, soil type and depth *D*. Because all N_{SPT} values are higher than 50, no N_{SPT}-*Vs* correlation is established. However, the best relation is established between *Vs* and the depths (Fig. 5*b*) as follow:

$$Vs = 18.72D + 275 \quad (2)$$

The site classification of the study area has been made in terms of average shear wave velocity of the top 30 m (*Vs30*) using Iranian code of practice (Standard No.2800) and National Earthquake Hazards Reduction Program (NEHRP). Table 2 presents the related site classes to these two classification system. Table 3 tabulates the site categories in Iranian code of practice provisions (Standard No.2800) and the corresponding NEHRP provisions classes. As seen in Table 2, all sites are placed in class II of the Standard No.2800 corresponding to class C of the NEHRP provisions.

4. Microtremor measurements and data analyses

Microtremor measurements were carried out at 85 sites covering all the accessible parts of the area (Fig. 6) employing the 24-bit digitizer 3-component seismometers of SARA instrument, model SL07 with GPS timing and recording memory. All stages for this work included the installation of the instruments and data recording were followed under the procedures introduced in the SESAME guidelines (Sesame, 2003). Horizontal-to-vertical spectral calculation was done by the procedure used in GEOPSY software. The procedure was carried out on the frequency range of 0 - 20 Hz, using 25- to 35-second non-overlapping time length, Konno and Ohmachi smoothing filter and removing time windows contaminated by non-stationary transient noises. Figure 7*a* shows a signal display with colored windows used for computing H/V matching with colors of individual H/V curves presented in Figure 7*b*.

Following up the guidelines criteria, the reliability of the H/V curves and the clarity and reliability of the H/V peaks were examined (see Bard et al., 2005 for details). Passing this QC, the verified frequencies were selected as the resonance frequencies. There is no consensus regarding the H/V amplitudes. Generally, it underestimates the

absolute values of the site amplification and is considered as a lower bound of the actual site amplification, so its application for engineering purposes is often not addressed.

4.1 Topology and spatial distribution of the H/V curves

The shapes of the H/V curves play a significant role while deriving the site effect indicators, i.e., resonance frequency *f* and amplification factor. Clear peaked curve occurs when the site under study has a significant velocity contrast (at least, approximately 4) at some depth. No-neat peak condition is very likely related to local subsurface structures, which may not exhibit any sharp velocity contrast at any depth, leading to low to moderate amplification (Konno and Ohmachi, 1998; Bonnefoy-Claudet, et al., 2009). Any other H/V shapes might be related to the subsurface geology or the irregular shapes of the basin (2D or 3D features).

Detailed study of the H/V data observed in Khash shows that the shapes of the H/V curves are not uniform. 12 H/V curves (18 percent of reliable data) do not show any clear peak, whereas, 69 curves (82 percent of reliable data) show at least one peak. Accordingly, in terms of peak condition, three major types of H/V curves were categorized, comprising the curves with: *a)* clear peaks; *b)* broad peaks; and *c)* flat/low amplification peaks, i.e. amplification below 2 (Fig. 8). There are a few instances indicating peaks of high frequency with industrial origins, like curve "*c1*" at f = 8.2 Hz. Figure 9 illustrates the spatial distribution of the various types of the H/V curves over the surficial geology map of the study area. Although, there is no robust data available to precisely justify such distribution, some conclusions can be made in terms of their impedance contrast. For example, the flat H/V curves are seen along western to south western parts on thin pebbly/gravelly sediments or even rocky hillsides, which resulted in low/no amplification regions due to low impedance contrast. The stations corresponding to the clear peaked curves have been mainly distributed at the center over a zone parallel to the valley on silty clay to silty sand sediments. From geometrical situation (i.e., the valley center) one can guess thicker sediments on bedrock that cause a higher impedance contrast. The H/V curves with broad peaks are appeared everywhere except for the western hillside and the central part. Again, considering the local geology/geometry related to a valley basin and the literature, these curves are likely located in the steeply dipping bedrock. Such broad peaks may also be due to the significant 2D or 3D variations in sediment–bedrock structure near the basin edges that generate a complex wavefield (diffracted body and surface waves) (Uebayashi, 2003; Cornou et al., 2003; Bonnefoy-Claudet et al., 2009).

In spite of the abovementioned general trends for the spatial distribution of the H/V curves over the study area, there exist a few scattered instances that contravene the trends. In other words, some H/V curves are randomly distributed over the area. For example, in the central part of the area, there exists a zone with no amplification. This may arise from any unknown subsurface topography. However, a meticulous attention was paid during extracting information from the H/V curves, especially for generating the site effect prediction maps. On this basis, some H/V curves were excluded for upcoming quantitative interpretation.

4.2 Site effects assessment

As previously mentioned, microtremor H/V technique is efficient for quantitative seismic microzonation, in urban areas. In the literature pertinent to site effects assessment and seismic microzonation, it is common to plot the distribution of the resonance frequency and site amplification factors as contour maps. Because there has been debate over the H/V amplification factor, only the map of iso-predominant period ($1 / f$) was built, using the triangulation interpolation techniques and the related amplitudes were presented by the size code circles (Fig. 10). The selected frequencies for contour intervals are based on what have proposed in Iranian Standard No.2800 (Table 4), according which the site classification has been done. The predominant period of the site ranges from 0.4 to 1.54 s in which the periods below 0.4 s (site class I) imparts 1%, the range of 0.4 – 0.5 s (site class II) imparts 4%, the range of 0.5 – 0.7 s (site class III) imparts 25%, and the periods above 0.7 s (site class IV) imparts 70%. Such variations do not show significant ascending/descending order. As Figure 10 shows, the quasi-amplitude value ranges from 1.8 to 7.0. The amplitudes higher than 5 are rare and have scattered over the basin.

4.3 Estimating Vs structure

Shallow shear velocity is traditionally determined with engineering surveys in boreholes, such as crosshole, downhole, and suspension logger surveys. As such methods are costly and invasive, there is a general trend to estimate *Vs* from microtremor observations. There are a number of array-based techniques for using microtremors to

deduce the shear wave velocity structure of a site. However, these techniques involve more complex equipments/operations and their analyses are tedious. As an alternative economic practice, having H/V data, we encouraged to examine H/V-based techniques. In this regard, we employed the program ModelHVSR. This is a Matlab tool used to either verify the existing geotechnical models by comparing theoretical H/V to the observed one, or invert the observed microtremors to derive most likely *Vs* profiles. It has been employed in a number of sites, for example: various sites in Croatia, Slovenia and Macedonia (Herak, 2008) and Jammu, India (Mahajan et al., 2012). It computes theoretical *Vs* and *Vp* amplification spectra of a layered visco-elastic model for vertically incident S- and P-waves, respectively. The model consists of a horizontally visco-elastic multi-layered soil column over a half space, whose layers are defined by six parameters: thickness (h), propagation velocity of the body wave (*Vs* and *Vp*), density (ρ), and the frequency dependent Q-factor (Qs and Qp) which controls the anelastic properties. The program inverts the observed H/V spectra by Monte Carlo perturbation of initial model within the user-bound defined parameters to obtain the best fitting family of models. The routine randomly perturbs model parameters as many times the user wish. After completing the iteration process, the best model is generated. The best model is the one whose theoretical H/V (H/V_{the}) most closely matches the observed one (H/V_{obs}), i.e. whose misfit function (*MF*) is the smallest, as:

$$MF = \Sigma\{[(H/V_{obs} - H/V_{the})2]*H/V_{obs}E\ , \qquad E \geq 0 \tag{3}$$

After the prescribed number of tries, one can check the confidence limits of the best model parameters found. Figure 11 represents H/V inversion results for station kh8 as an example and describes some related aspects.

From all H/V measurement stations at Khash basin, only 11 S-wave profiles indicating low misfit functions were chosen (Fig. 12*a*) and the low fit ones were rejected. To check the reliability of the results, we made a comparison between the *Vs*'s – depths relation of these models and the downhole ones (Fig. 12*b*). In a general trend, the *Vs* values acquired by ModelHVSR modeling of microtremors are lower than 19% of the values acquired by downhole surveys. However, such differences are acceptable for a *Vs* modeling as seen in other modeling methods and have no significant influence on microzonation or similar studies, especially when used alongside other geophysical or geotechnical data. For example, as seen for downhole data, all sites are classified as class II of Standard No.2800 corresponding to class C of the NEHRP provisions, except for stations kh28 and kh8 that are classified as classes III or D of the two systems. The analyses lead us to conclude that the sites having high H/V amplitudes and clear peaked curves get better results with low misfit functions.

5. Summary and Conclusions

This study is the first to describe the effects of local geological condition on seismic ground motion in Khash area, south east of Iran. A simple geological study indicated that the city is placed on the core of an eroded anticline, but the limited data available were not able to define the geology of the site. So, a reconnaissance campaign—including geological, geotechnical and seismic downhole surveys— was conducted. Information from six geotechnical drillings and sampling together with the geological interpretation gave a general description of the surface and subsurface of the area. However, the drillings suffer from two shortages; a) due to financial problems, drilled boreholes were not sufficient for a detailed subsurface exploration and did not reach the bedrock; and b) urban area limitations led to an uneven distribution of boreholes on the basin. The prepared surface geology map within the Khash valley shows that silty clayey to silty sandy sediments cover a great majority of the central basin and the vicinity hillsides are covered by gravelly to cobbly materials. Two other major geological units were inferred as well, comprising bedrock that varies from sandstone to shale layers at different localities, and a dense and cemented silty layer -chalky layer underlain by softer layers- has drawn along a narrow band in the northern parts towards the south of the city. Six seismic downhole surveys in pre-drilled geotechnical boreholes showed that the S-wave velocities vary in the range of 155-800 m/s. The best correlation between *Vs* and other soil indexes was established for the variations of *Vs* with the depths as: $Vs = 18.72\ D + 275$. The site classification of the study area was done in terms of average shear wave velocity of the top 30 m (*Vs30*); accordingly, the site entirely classified as class II of the Iranian Standard 2800 corresponding to class C of the NEHRP provisions.

For site effect purposes, microtremor observations were carried out at 85 stations. A detailed analysis of microtremor data submitted three major topologies of H/V curves, included clear peaked curves, curves with broad peak(s), and flat curves or curves with amplifications below 2. The stations corresponding to clear peaked curves have been

mainly distributed over a zone parallel to the valley on silty clay to silty sand sediments. Except for the western and central parts, the broad curves appear everywhere that probably reveals dipping bedrock, considering inferred local geology in the basin of a valley. The flat H/V curves are located in the western and south western parts on thin pebbly/gravelly sediments or even hilly rock regions. In central basin, there exists a zone of no amplification, as well. A few scattered instances are randomly distributed over the area, which do not conform to the mentioned trend. This may arise from any unknown subsurface structures.

In this basin, surface geology is not able to fully justify the distribution patterns of the various shapes of H/V curves on a site. One conclusion is that the underground geological factors are more dominant rather than surface geology effects. However, some conclusions can be made in terms of their impedance contrast. For example, the occurrence of the flat H/V curves on thin pebbly/gravelly sediments and rocky hillsides can be justified by the low impedance contrast pertinent to such regions. A conclusion for the existence of stations corresponding to the clear peaked curves at the valley center is provided by considering their location on soft sediments as well as geometrical situation; one can guess that thicker sediments on bedrock might cause a high impedance contrast. As some steeply dipping bedrock can be imagined for the regions between the valley center and the adjacent heights, the existence of H/V curves with broad peaks maybe satisfied. However, further data like earthquake or geotechnical data should be employed to verify such deductions. Unfortunately, such information is not currently available.

The iso-predominant period map of sediments shows a variation in the range of 0.4 to1.54 s in which the periods below 0.4 s (site class I) imparts 1%, the range of 0.4 – 0.5 s (site class II) imparts 4%, the range of 0.5 – 0.7 s (site class III) imparts 25%, and the periods above 0.7 s (site class IV) imparts 70%. As seen, there is no good relation between these classes and what has obtained by downholes, which classified the whole site as class II (C). One conclusion is that the *Vs30* is not sufficient for site amplification, as *Vs30* does not take into account impedance contrasts, as mentioned by other authors (Gallipoli et al., 2009; Castellaro, et. al, 2008).

The *Vs* structures of the basin have been estimated on the basis of H/V data concerning a simplified hypothesis pertinent to the nature of the noise wave-field: the noise H/V is basically composed by the body waves. On this basis, 11 soil models were derived by ModelHVSR that are comparable with downhole results. These models are related to the sites having rather high amplitudes and clear peaked curves. Thus, it can be concluded that this technique can be used for evaluating site effects in areas with high velocity contrast.

It is proposed that an ambient noise array program combined with a denser grid of H/V data would be suitable to define the spatial distributions of the predominant periods and to provide more accurate estimates of the subsoil velocity profiles in the whole basin. An inversion analysis considering surface waves, which may improve our insight about the area, might also be proposed for future studies. If earthquake or other geophysical data are available in the future, these would be idealistic to verify the microtremor data and to grasp the real amplification of the ground motion.

Acknowledgments

The authors would like to thank Mr. Rouzbeh Yazdanfar whose insightful comments helped a lot to improve the analyses. We also thank Mr. Reza Eftekharnia and Mr. Seyyed Hamid Fazeli for their assistance with microtremors measuring and drawing the maps.

References

Anbazhagan, P. and Sitharam, T.G. (2009). Spatial variability of the depth of weathered and engineering bedrock using multichannel analysis of surface wave method, Pure appl. geophys 166, 409–428.

Apostolidis, P.I., Raptakis, D.G., Pandi, K.K., Manakou, M.V., and Pitilakis, K.D. (2006). Definition of subsoil structure and preliminary ground response in Aigion city (Greece) using microtremor and earthquakes, Soil Dynamics and Earthquake Engineering, 26, 922–940.

Bard, P.-Y. (1998). Microtremor measurements: a tool for site effect estimation? Proceedings of the second international symposium on the effects of surface geology on seismic motion, Vol. 3, Yokohama, Japan, pp. 1251-1279, Balkema: Rotterdam, Yokohama, Japan.

Bard, P.-Y. and SESAME-Team. (2005). Guidelines for the implementation of the H/V spectral ratio technique

on ambient vibrations–measurements, processing and interpretations, SESAME European research project EVG1-CT-2000–00026, deliverable D23.12, 2005, available at http://sesamefp5.obs.ujf-grenoble.fr.

Bonnefoy-Claudet, S., Cotton, F., and Bard, P.-Y. (2006). The nature of noise wavefield and its applications for site effects studies. A literature review, Earth.-Sci. rev., 79, 205–227.

Bonnefoy-Claudet, S., Baize, S., Bonilla, L.F., Berge-Thierry, C., Pasten, C., Campos, J., Volent, P., and Verdugo, R. (2009). Site effect evaluation in the basin of Santiago de Chile using ambient noise measurements, Geophysical Journal International 176, 925–937.

Borcherdt, R.D. (1970). Effects of local geology on ground motion near San Francisco Bay, Bulletin of the Seismological Society of America, 60, 29–61.

BSSC. (2003). NEHRP recommended provisions for seismic regulations for new buildings and other structures (FEMA 450), Building Seismic Safety Council for the Federal Emergency Management Agency, Washington, DC.

Castellaro, S., Mugaria, F., and Rossi, P.L. (2008). Vs30: Proxy for Seismic Amplification? Seismological Research Letters, Vol. 79, No. 4, 540-543.

Cornou, C., Bard, P.-Y., and Dietrich, M. (2003). Contribution of dense array analysis to the identification and quantification of basin-edge-induced waves, Part I: Methodology, Bulletin of the Seismological Society of America, 93(6), 2604–2623.

Delgado, J., López Casado C., Estévez, A., Giner, J., Cuenca, A., and Molina, S. (2000). Mapping soft soils in the Segura river valley (SE Spain): a case study of microtremors as an exploration tool, Journal of Applied Geophysics 45, 19–32.

Fäh, D., Kind, F., and Giardini D. (2003). Inversion of local S-wave velocity structures from average H/V ratios, and their use for the estimation of site-effects, Journal of Seismology 7, 449–467.

Field, E.H. and Jacob, K.H. (1995). A comparison and test of various site-response estimation techniques, including three that are not reference-site dependent, Bulletin of the Seismological Society of America, 85, 1127–43.

Field, E.H. and Jacob, K.H. (1990). The theoretical response of sedimentary layers to ambient seismic noise, Geophys. Res. Lett. 20(04), 2925-2928.

Gallipoli, M.R., and Mucciarelli, N. (2009). Comparison of Site Classification from *VS30*, *VS10*, and HVSR in Italy, Bulletin of the Seismological Society of America, 99, 1, pp. 340–351.

Ghayamghamian, M.R., and Hisada, Y. (2007). Near-fault strong motion complexity of the 2003 Bam earthquake (Iran) and low-frequency ground motion simulation, Geophysical Journal International, 170, 679-686.

Herak, M. (2008). ModelHVSR–A Matlab® tool to model horizontal-to-vertical spectral ratio of ambient noise, Computer & Geosciences, 34, 1514-1526.

Holzer, T.L., Padovani, A.C., Bennett, M. J., T.E., Noce, T.E., and Tinsely, J.C. (2005). Mapping Vs30 site classes, Earthquake Spectra, 21, 335-370.

Ibs-Von Seht, M. and Wohlenberg, J. (1999). Microtremor measurements used to map thickness of soft soil sediments, Bulletin of Seismological Society of America, 89, 250–259.

Iranian code of practice for seismic resistant design of building, 3rd revision (Standard No. 2800). (2005). Building and Housing Research Center.

Kearey P., Brooks M., and Hill I. (2002). An introduction to geophysical exploration, Publ. John Wiley & Sons.

Konno, K. and Ohmachi, T. (1998). Ground-motion characteristics estimated from spectral ratio between horizontal and vertical components of microtremor, Bulletin of the Seismological Society of America, 88**(**1) 228–241.

Kramer, S.L. (1996). *Geotechnical Earthquake Engineering*, Publ. Prentice Hall.

Lachet, C., Bard, P.-Y. (1994). Numerical and theoretical investigations on the possibilities and limitations of Nakamura's technique, J. Phys. Earth, 42, 377-397.

Lang, D.H., and Schwarz, J. (2006) Instrumental subsoil classification of Californian strong-motion sites based on single-station measurements, Eighth U.S. National Conference on Earthquake Engineering, San Francisco, United States.

Lermo, J., and Chavez-Garcia, F.J. (1993). Site effects evaluation using spectral ratios with only one station, Bulletin of the Seismological Society of America, 83, 1574–1594.

Luna, R. and Jadi, H. (2000) Determination of dynamic soil properties using geophysical methods, Proceedings of the first international conference on the application of geophysical and NDT methodologies to transportation facilities and infrastructure, St. Louis, MO.

Mahajan, A.K., Mundepi, A.K., Neetu Chauhan, Jasrotia, A.S., Nitesh Rai., and Gachhayat, T.K. (2012). Active seismic and passive microtremor HVSR for assessing site effects in Jammu city, NW Himalaya, India—A case study, Journal of Applied Geoph., 77, 51-62.

Nakamura, Y. (1989). Real time information systems for seismic hazards mitigation UrEDAS, HERAS and PIC, Quarterly Report of RTRI, 37(3), 112-127.

Nakamura, Y. (1997) Seismic vulnerability indices for ground and structures using microtremor, World congress on railway research in Florence, Italy.

Nogoshi, M. and Igarashi, T. (1971). On the amplitude characteristics of microtremor, J Seism Soc Japan, 24**,** 26–40, In Japanese with English abstract.

Parolai, S., Bormann, P., and Milkereit, C. (2002). New relationship between Vs, thickness of sediments, and resonance frequency calculated by the H/V ratio of seismic noise for the Cologne area (Germany), Bulletin of the Seismological Society of America 92(6), 2521–2527.

Parolai, S. and Galiana-Merino, J. J. (2006). Effects of transient seismic noise on estimates of H/V spectral ratios, Bulletin of the Seismological Society of America, 96(1), 228–236.

Picozzi, M., Strollo, A., Parolai, S., Durukal, E., Özel, O., Karabulut, S., Zschau, J., and Erdik, M. (2009). Site characterization by seismic noise in Istanbul, Turkey, Soil dynamics and earthquake engineering 29 (3), 469–482.

Shahrabi, M. (1995). Explanatory text of the Khash Quadrangle map, 1:250000, GSI Geological Quadrangle NO. L.12.

Uebayashi, H. (2003). Extrapolation of irregular subsurface structures using the Horizontal-to-Vertical Spectral Ratio of long-period microtremors, Bulletin of the Seismological Society of America, 93(2), 570-582.

Williams, R.A., Wood, S., Stephenson, W.J., Odum, J.K., Meremonte, M.E., Street, R., and Worley, D. (2003). Surface seismic refraction/reflection measurement determinations of potential site resonances and the areal uniformity of NEHRP site class D in Memphis, Tennessee, Earthquake Spectra, 19, 159-189.

Woods, R. D. (1978). Measurement of dynamic soil properties, Proceedings of the ASCE geotechnical engineering division specialty conference on earthquake engineering and soil dynamics, ASCE, Vol I, 91–178.

Table 1. Shear strength parameter of soil columns of depths 2-5 m.

Borehole No.	BH1	BH2	BH3	BH4	BH5	BH6
φ (degree)	30-23	27-33	39-36	42-40	-	40-37
c (kgf/cm^2)	0.30-0.23	0.31-0.20	0.06-0.12	0.03-0.01	-	0.03

Table 2. Site categories in Iranian code of practice and NEHRP provisions.

Borehole	*Vs30*	Site class	
	(m/s)	Standard No.2800	NEHRP
BH1	411	II	C
BH2	381	II	C
BH3	448	II	C
BH4	530	II	C
BH5	520	II	C
BH6	725	II	C

Table 3. Site categories in Iranian code of practice (Standard No.2800).

Group	**Constituent materials**	
I (B)	(a) Igneous rocks, hard and stiff sedimentary rocks and massive metamorphic rocks	*Vs30* > 750
	(b) Conglomerate beds, stiff soil with over 30m in thickness	
II (C)	(a) Loose igneous rocks, friable sedimentary rocks, foliated metamorphic rocks	375 < *Vs30* < 750
	(b) Stiff soil with thickness less than 30 m	
III (D)	(a) Rocks disintegrated by weathering	175 < *Vs30* < 375
	(b) Medium compaction soils, beds of gravel and sand with medium intragranular cementation bond	
IV (E)	(a) Soft and wet deposits resulted from high level of water table	*Vs30* < 175
	(b) Any kind of soil containing a 6-m high clay layer less than 175 with cementation index over 20	

The capital letters in parentheses indicate corresponding NEHRP provisions classes.

Table 4. Standard 2800 site classes related to T period range.

T (s)	<0.4	0.4 - 0.5	0.50 - 0.7	0.7<
Site class	I	II	III	IV

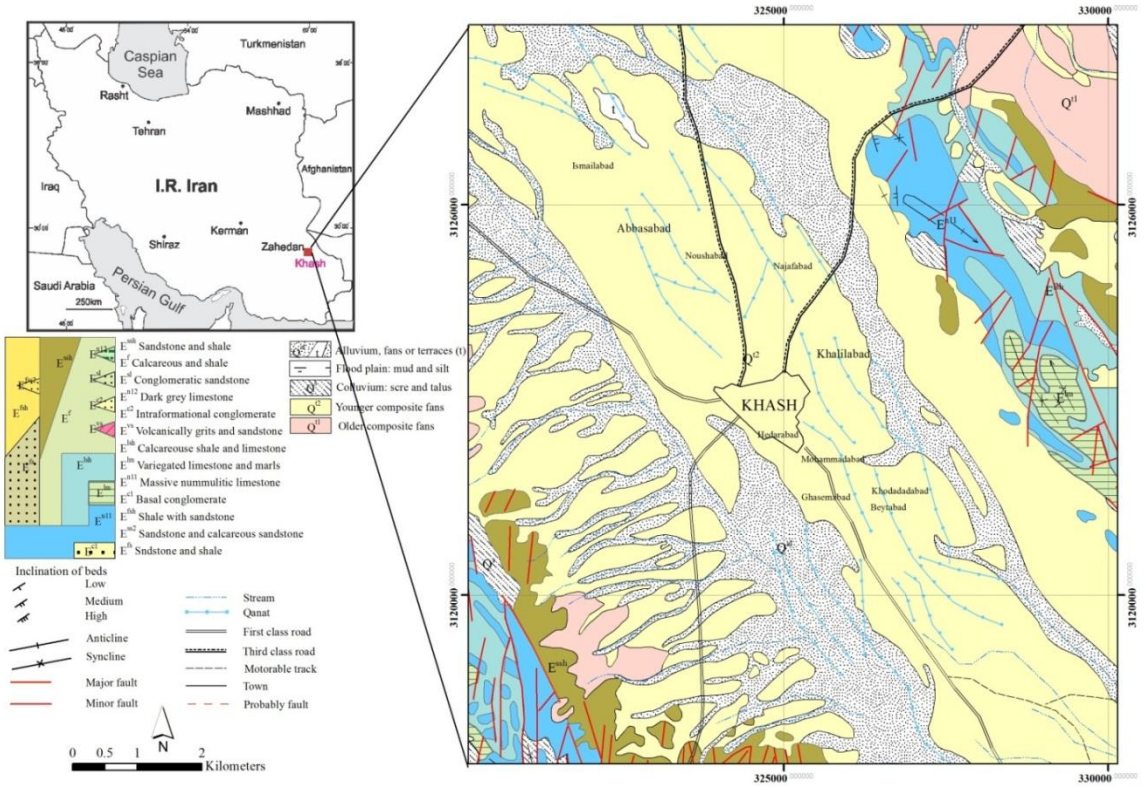

Figure 1.Geological map of Khash area (redrawn from Shahrabi, 1995)

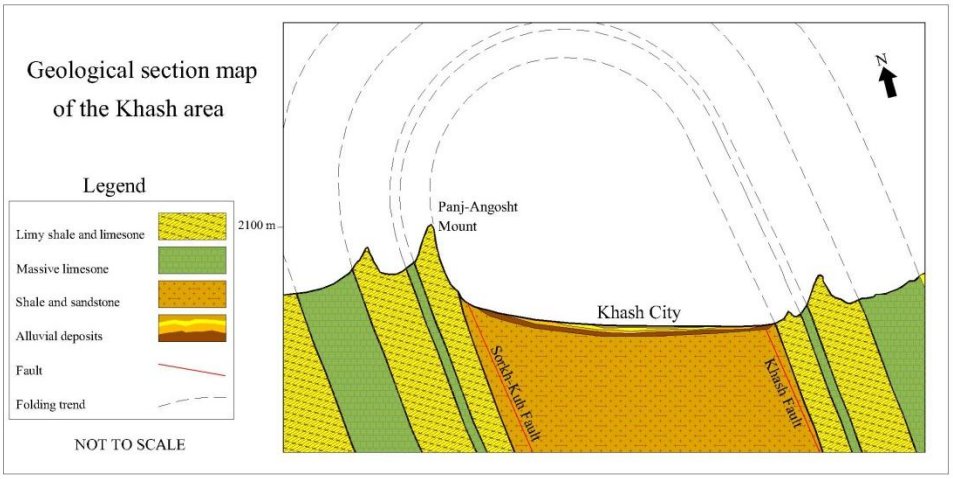

Figure 2. Simplified geological section map of the Khash area along the west-east of the valley

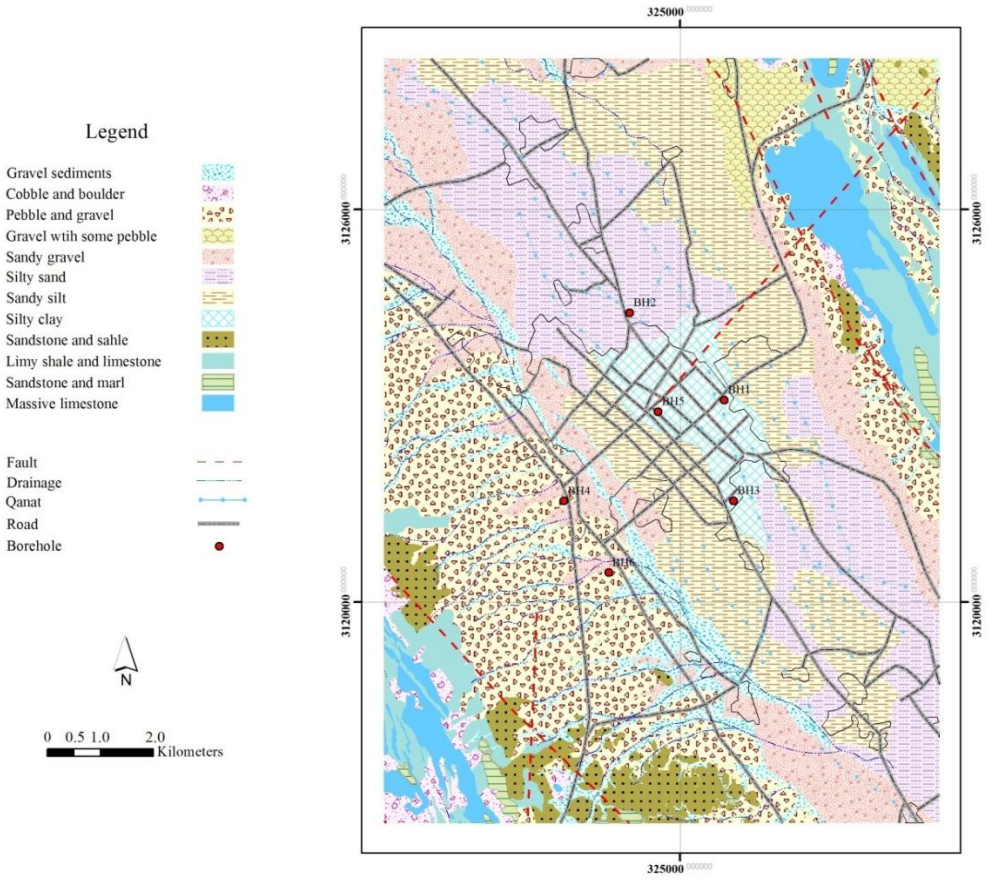

Figure 3. The layout of boreholes on the surface soil map of Khash basin. The soil texture map was derived on the basis of the borehole logs and the geological investigations.

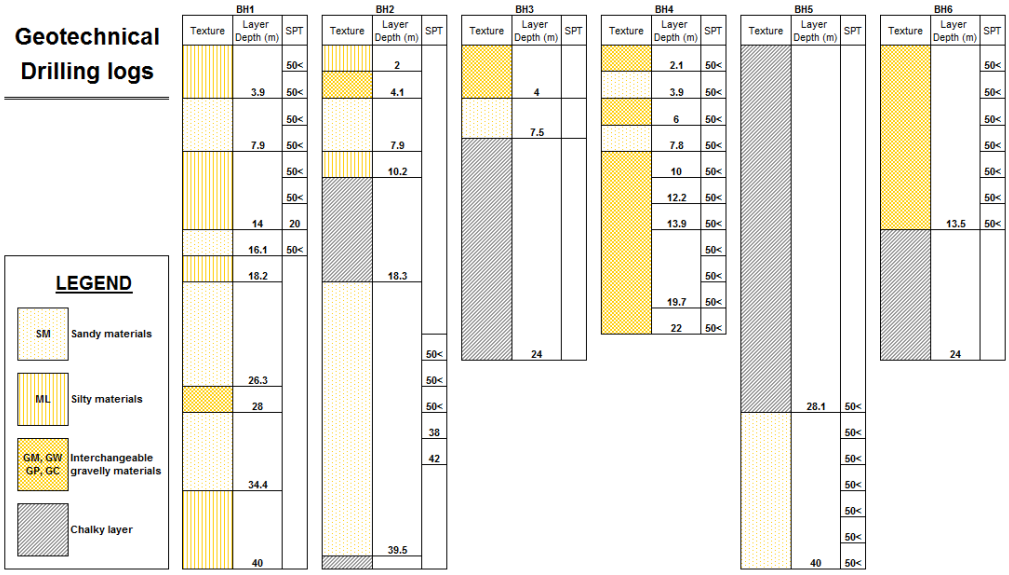

Figure 4. Geotechnical drilling logs for the six boreholes at Khash basin.

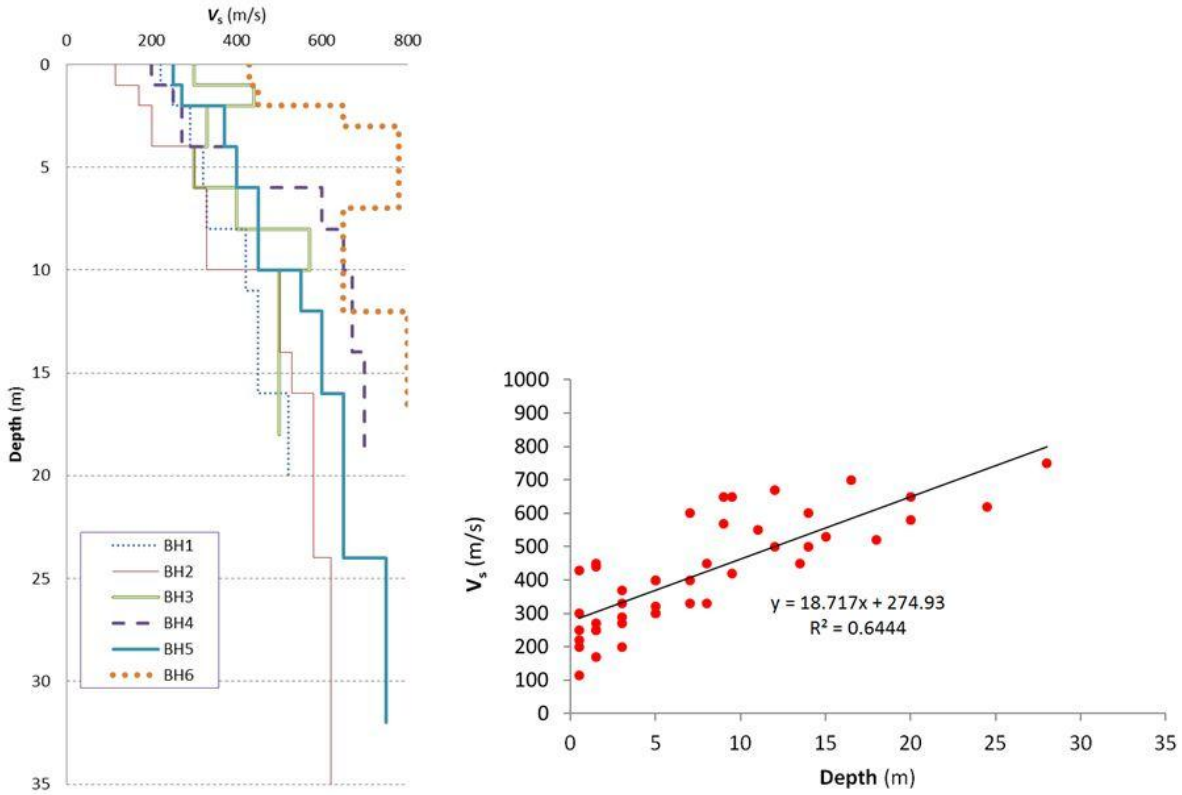

Figure 5. *Left: Vs* profiles form downhole surveys. *Right*: Depths versus the *Vs*'s obtained from seismic downhole logging to derive equation 3.

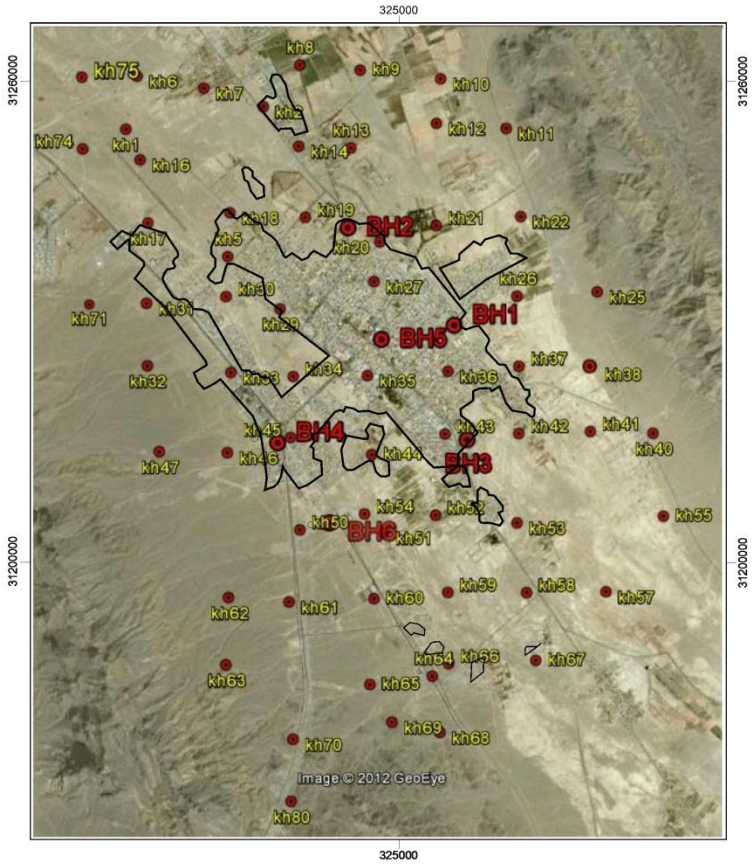

Figure 6. Location of the microtremor stations on the Google Earth image. The stations in red characters belong to the boreholes. Black lines are the city borders.

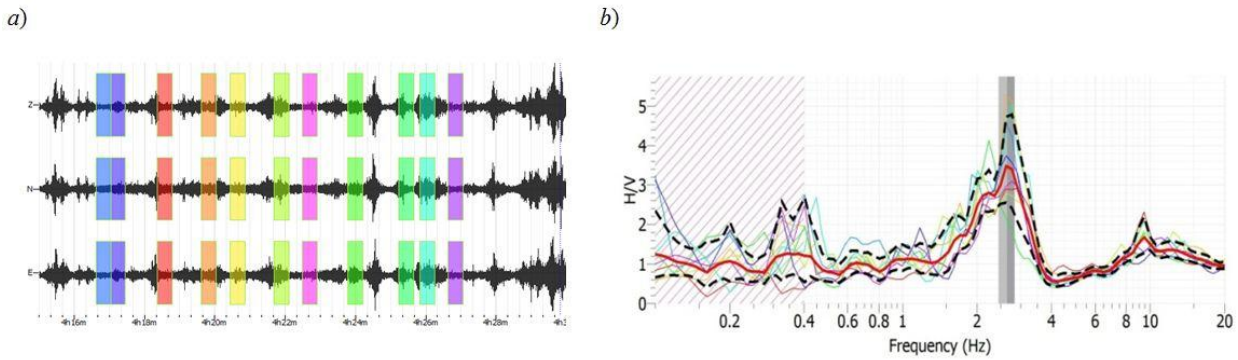

Figure 7. a) Processing scheme: vertical (Z), north-south (N) and east-west (E) components with colored windows used for computing H/V matching with colors of individual H/V curves presented in the right figure. b) The red curve represents H/V mean curve and the two dashed lines represent H/V standard deviations. The gray strip represents the averaged peak frequency. Frequencies lower than the minimum reliable frequency are hachured in red.

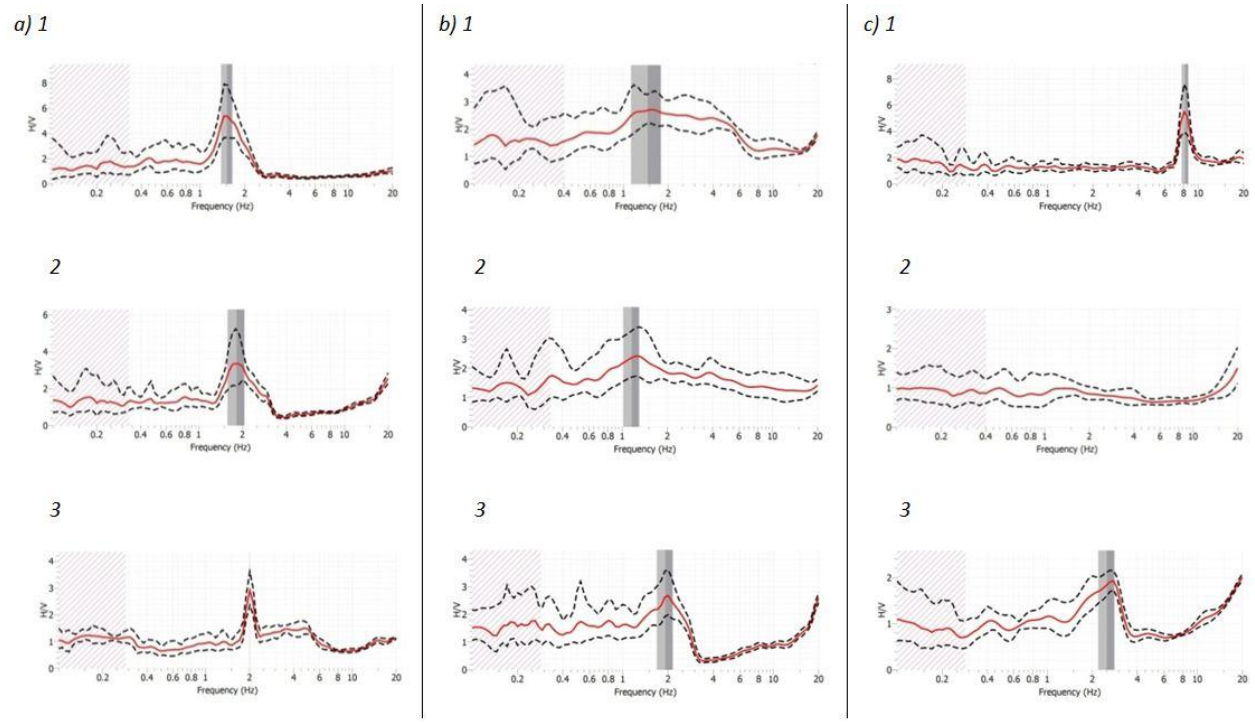

Figure 8. Topology of the H/V curves observed in Khash area: *a)* clear peaked curves; *b)* broad peaked curves; and *c)* flat/low amplification peaked curves. Herein the gray bands do not necessarily indicate the resonance frequencies.

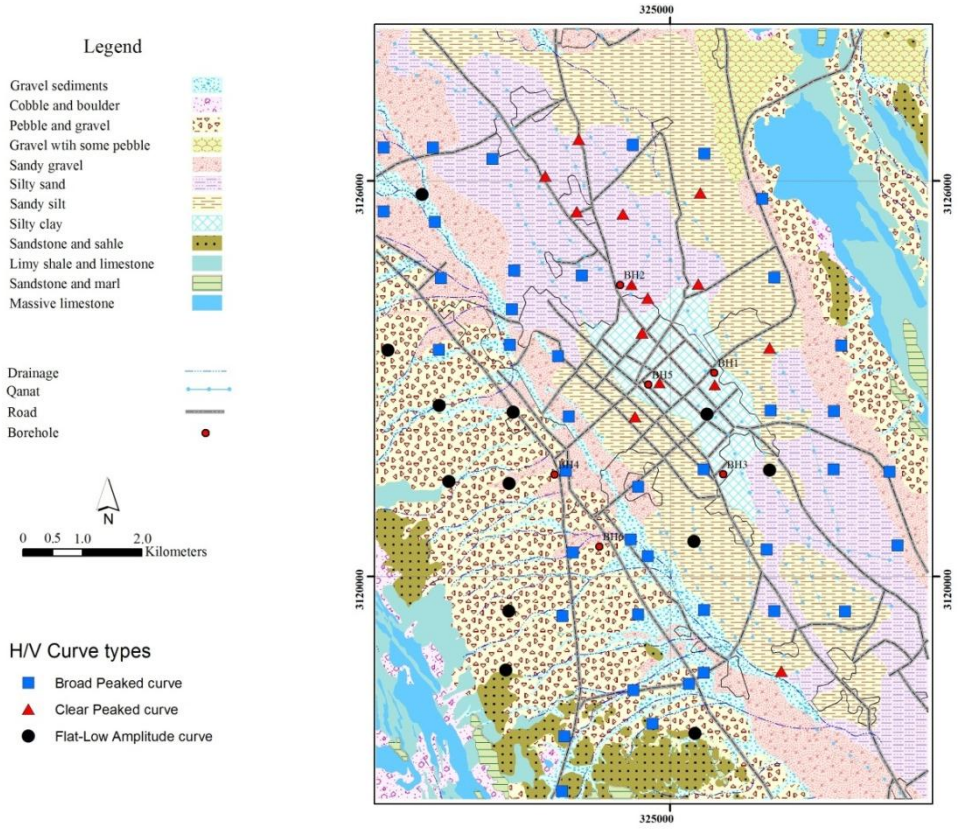

Figure 9. Spatial distribution of the various types of the H/V curves in the basin of Khash over the surface geology map.

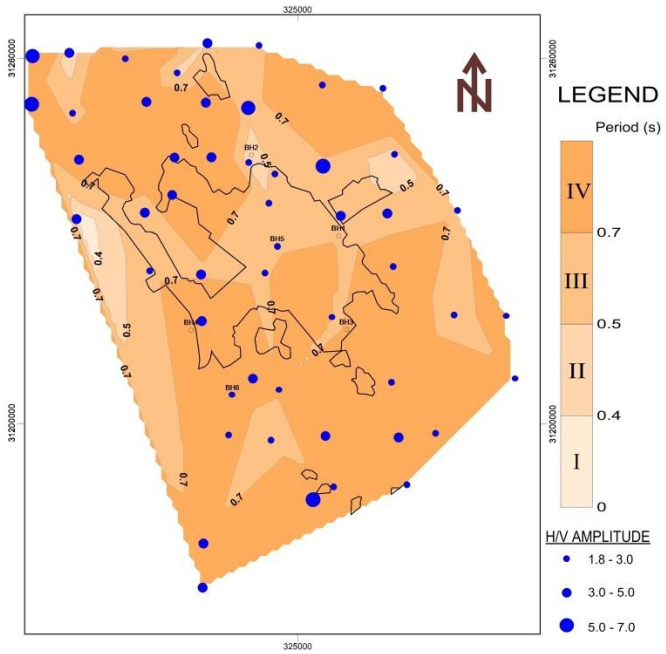

Figure 10. Site period map accompanied by site classes (roman numerals in the scale bar) zones corresponding to Iranian Standard No.2800 classification. Circles display H/V amplitude values for H/V curves.

a)

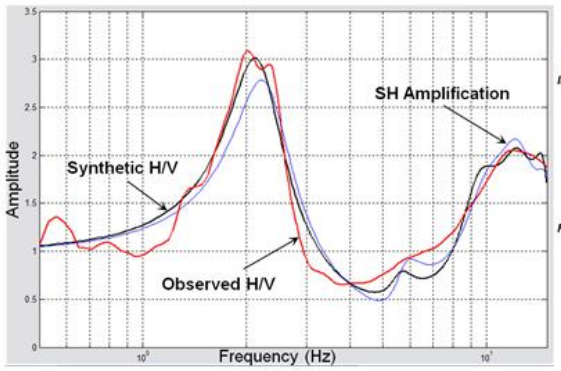

Layer	Vp (m/s)	Vs (m/s)	ρ (g/cm³)	H (m)	Qp	Qs
Initial model (k=0.25, DAF=1.26)						
1	400	150	1.7	1*	10	5
2	600	300	1.75	8*	18	8
3	1000	400	1.8	8*	30	12
4	1400	500	1.85	11*	45	15
5	1800	600	1.9	11*	60	20
	3000*	800*	2.1*	999*	999*	999*
Final model (k=0.25, DAF=2.21 [2.07-2.27]); After 2 * 10,000 perturbation						
1	349 [293-413]	150 [151-171]	1.91 [1.7-2.0]	1*	9 [7.81-11.1]	5 [4.14-5.87]
2	676 [587-749]	175 [160-191]	1.7 [1.7-1.88]	8*	21 [17.6-24.0]	10 [8.12-11.4]
3	1013 [398-1235]	290 [264-339]	1.7 [1.7-1.9]	8*	44 [34.5-47.7]	27 [20.9-30]
4	606 [548-681]	260 [242-284]	1.72 [1.7-1.88]	11*	45 [41.1-54.7]	30 [20.7-30]
5	1273 [1086-1483]	512 [445-559]	1.84 [1.7-2]	11*	61 [48.1-72.4]	30 [25.5-30.0]
	3000*	800*	2.1*	999*	999*	999*

b)

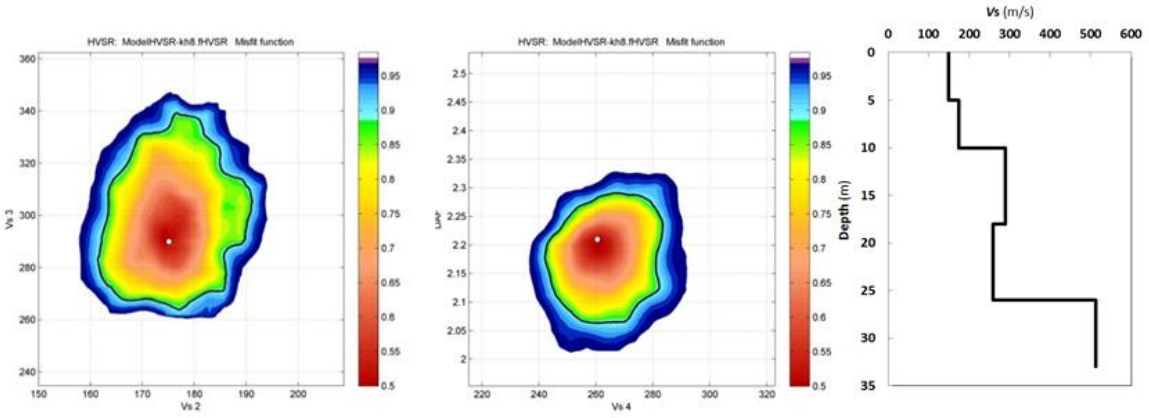

Figure 11. Modeling of observed H/V—example from station kh8. a) *Left side*: red line is observed H/V (from microtremor measurements), blue one is theoretical H/V of starting model, and black is (synthetic) H/V of final model that best fits observed data. *Right side*: initial model (related to red line) and final model (related to black line) of a 5-layer soil column after 2 * 10 000 perturbation. Asterisk (*) denotes fixed parameters. Values in square brackets are 90% confidence limits for final parameters. Amplification (dynamic amplification factor, DAF) is computed for an earthquake of M=6.5, depth=20 km, distance=10 km, and percentage of rock on the ray-path=90%. b) *Left side*: two cuts through misfit space parallel to *Vs* in layers 3 and 2, and DAF and *Vs* in layer 4 of final model. Black enclosed curves are 90% confidence limits. Colorbars are calibrated in terms of confidence levels. Best solutions (*Vs*2 = 175 m/s, *Vs*3 = 290 m/s, and *Vs*4 = 260m/s, DAF = 2.21) are indicated by small white circles. *Right side*: final shear velocity model for station kh8 at Khash basin.

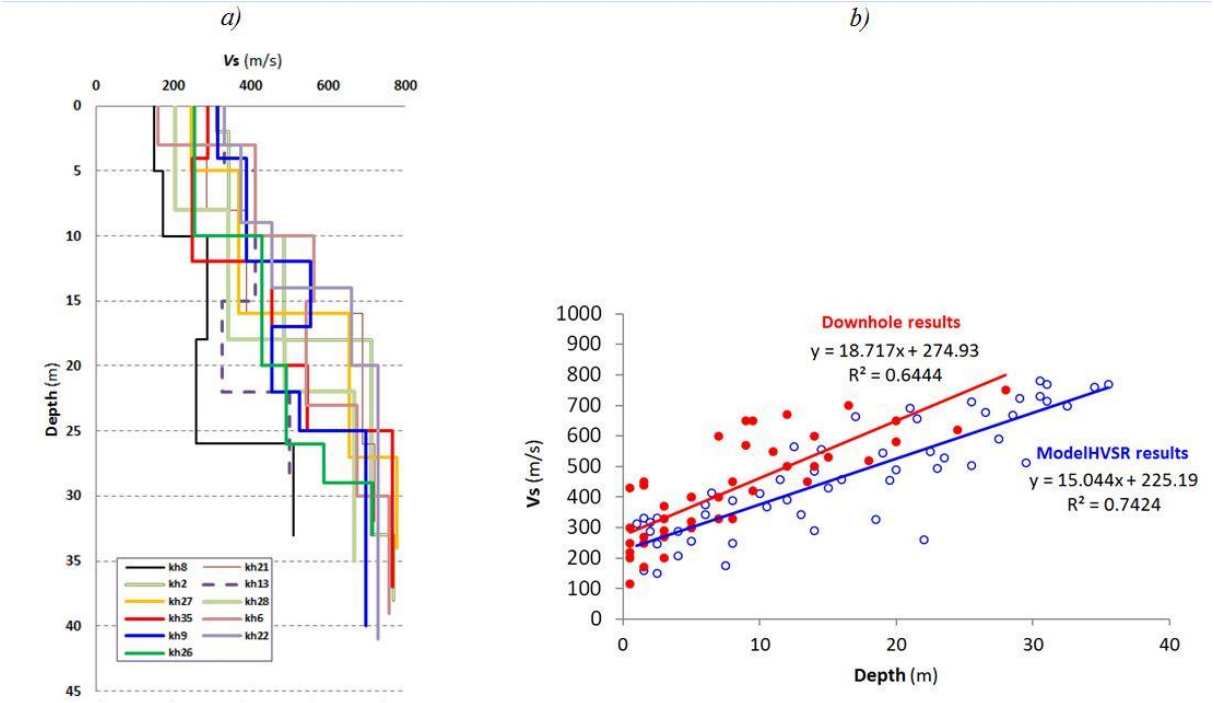

Figure 12. a) *Vs* profiles obtained by ModelHVSR modeling of microtremors for 11 stations. b) The comparison between seismic downhole and ModelHVSR modeling results.